ARMA 16-691

Determination of Maximum Horizontal Field Stress from Microseismic Focal Mechanisms – A Deterministic Approach

Agharazi, A
MicroSeismic Inc., Houston, Texas, USA

This paper was prepared for presentation at the 50th US Rock Mechanics / Geomechanics Symposium held in Houston, Texas, USA, 26-29 June 2016. This paper was selected for presentation at the symposium by an ARMA Technical Program Committee based on a technical and critical review of the paper by a minimum of two technical reviewers. The material, as presented, does not necessarily reflect any position of ARMA, its officers, or members. Electronic reproduction, distribution, or storage of any part of this paper for commercial purposes without the written consent of ARMA is prohibited. Permission to reproduce in print is restricted to an abstract of not more than 200 words; illustrations may not be copied. The abstract must contain conspicuous acknowledgement of where and by whom the paper was presented.

ABSTRACT: The state of field stresses is an important factor in the design and execution of hydraulic fracturing treatments. The absolute and relative magnitudes of horizontal stresses directly affect the minimum treatment horsepower requirement and the final stimulation pattern. While the minimum horizontal stress (σ_{hmin}) can be directly measured by a mini-frac or a leakoff test, there is no direct means to measure the magnitude of maximum horizontal stress (σ_{Hmax}). In this paper, we introduce a new method for determination of σ_{Hmax} direction and magnitude from microseismic focal mechanisms induced by hydraulic fracturing treatments. The focal mechanisms that meet a certain criterion are used to first determine the σ_{Hmax} direction. Knowing the direction of horizontal stresses, the reference coordinate system of principal stresses is formed by assuming the vertical stress as a principal stress. The normalized magnitude of σ_{Hmax} is then calculated for each qualifying focal mechanism as a function of normalized σ_{hmin} magnitude. The undisturbed σ_{Hmax} magnitude is estimated by interpretation of calculated σ_{Hmax} magnitudes for all focal mechanisms. The method was used to estimate direction and magnitude of σ_{Hmax} for two projects in the Marcellus Shale, located approximately 30 miles away from one another.

1. INTRODUCTION

The state of stress in a formation can be characterized by direction and magnitude of the three principal stresses. For close-to-surface projects, where undisturbed rock is accessible, techniques such as over-coring, flat jack test, hydraulic fracturing, and borehole slotter (Jaeger et al., 2008, Amadei and Stephansson, 1997) can be used to measure the stress magnitudes at the study region. In the case of unconventional reservoirs, however, access to the undisturbed rock is very limited, and most conventional stress measurement techniques cannot be applied. A common assumption in these cases is that the vertical stress is a principal stress whose magnitude is determined by calculating the weight of overburden rock from density logs. This assumption holds true in most cases, considering the high depth of unconventional reservoirs, except for cases where a geological feature such as a fault or fold changes the state of stress locally. Given the orthogonality of principal stresses, this assumption requires that the other two principal stresses be horizontal. Thus, the problem of determining the field stresses is reduced to finding the direction and magnitude of horizontal stresses.

While there are several techniques, such as a mini-frac test, leakoff test, and extended leakoff test, to directly measure the magnitude of minimum horizontal stress (σ_{hmin}) (Zoback, 2010), there is no direct and easy way to measure the magnitude of maximum horizontal stress (σ_{Hmax}). The analysis of borehole breakouts using the Kirsch equations for stresses around a circular hole can provide insights into the σ_{Hmax} direction and magnitude (Zoback, 2010). The same set of equations can also be used to back-calculate σ_{Hmax} magnitude from hydraulic fracturing of un-cased and un-cemented wells (Zoback, 2010, Amadei and Stephansson, 1997). However, this method is not applicable in most horizontal wells drilled in unconventional reservoirs, mainly because these wells commonly have casing and are cemented. Sinha et al. (2008) reported the application of borehole sonic data for estimation of horizontal stresses.

The stress inversion technique, frequently used by seismologists to determine the stresses associated with an earthquake focal mechanism, has also been used by some authors to estimate the formation stresses from focal mechanisms of microseismic events induced by hydraulic fracturing stimulations (Neuhaus et al. 2012, Sasaki and Kaieda, 2002). In this method, usually a grid-search approach is utilized to find a stress model, including three principal directions and a ratio of stresses, that best fits the observed slips on all study fault planes, or fracture planes in the case of microseismic events (Michael 1984, Angelier 1990, Gephart and

Forsyth 1984). The main difference between various versions of this method is the residual function that is to be minimized during the inversion process. A fundamental assumption in this method is that all fault planes are under the same stress state (uniform stresses) (Sasaki and Kaieda, 2002), so a best-fit solution can be found that represents the field stresses. However, an induced hydraulic fracture affects field stresses and changes the magnitude and even direction of stresses within the treated region. Numerical studies show that at least three different stress zones can theoretically be identified around a vertical hydraulic fracture (Agharazi et al. 2013, Nagel et al. 2013): i) the shear zone at the leading edge of the propagating fracture with rotated stress directions and modified stress magnitudes, ii) the stress-shadow zone on either side of the fracture with increased stress magnitude in the direction perpendicular to the fracture plane, and iii) the undisturbed zone outside of the previous two zones with stress directions and magnitudes representing the initial or undisturbed field stresses.

Applying the stress inversion method to a set of microseismic focal mechanisms that belong to different stress regimes adds a significant uncertainty to the estimated stress parameters and results in a non-representative stress model. The vertical scatter of microseismic hypocenters and variation of stress magnitudes with depth is also another source of error if the applied equations are not normalized by depth. This method is also unable to identify unqualified and incompatible focal mechanisms that are not eligible for stress inversion. The unqualified focal mechanisms are associated with the fractures whose dip or strike are parallel to a principal stress direction, and must be eliminated from stress inversion (they fit into unlimited number of solutions). The incompatible events, on the other hand, are associated with the inherent ambiguity in the moment tensor solution (auxiliary plane versus real plane) or the noise-related errors (polarity in rake vector direction) and need to be identified and properly addressed before proceeding to stress analysis. Fitting a stress model to a microseismic data set that contains unqualified and incompatible focal mechanisms results in a significant error in the estimated stress directions and ratio.

In this paper, we introduce a deterministic method for estimation of maximum horizontal stress direction and magnitude based on microseismic focal mechanisms observed during hydraulic fracturing stimulation of unconventional reservoirs. In this method, σ_{Hmax} direction is first determined and the reference coordinate system of principal stresses is established. The magnitude of σ_{Hmax} is then calculated for each qualified microseismic focal mechanism. The undisturbed maximum horizontal stress magnitude is then estimated by interpretation of calculated stresses for each event. Therefore, the field stress tensor can be determined if the magnitudes of vertical and minimum horizontal stresses are known. The suggested method is used to back-calculate field σ_{Hmax} direction and magnitude for two Marcellus projects.

2. SEISMIC MOMENT TENSOR AND FOCAL MECHANISM

The seismic moment tensor is a mathematical description of deformation mechanisms in the immediate vicinity of a seismic source. It characterizes the seismic event magnitude, fracture type (e.g., shear, tensile), and fracture orientation. The seismic moment tensor is a second order tensor with nine components shown by a 6×6 matrix as follows:

$$M = M_o \begin{bmatrix} M_{11} & M_{12} & M_{13} \\ M_{21} & M_{22} & M_{23} \\ M_{31} & M_{32} & M_{33} \end{bmatrix} \quad (1)$$

where M_o is the seismic moment and M_{ij} components represent force couples composed of opposing unit forces pointing in the i-direction, separated by an infinitesimal distance in the j-direction. For angular momentum conservation, the condition $M_{ij} = M_{ji}$ should be satisfied, so the moment tensor is symmetric with just six independent components. A particularly simple moment tensor is the so-called double couple (DC), which describes the radiation pattern associated with a pure slip on a fracture plane. The DC moment tensor is represented by two equal, non-zero, off-diagonal components.

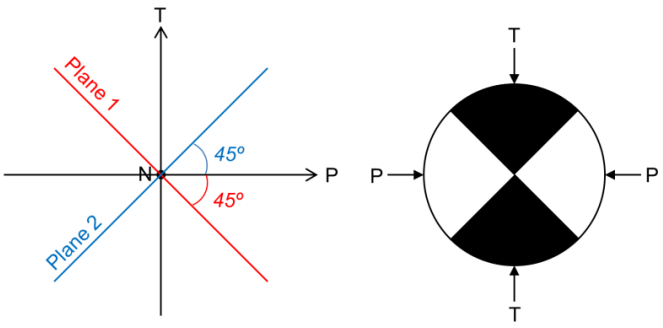

Figure 1: Three orthogonal eigenvectors of moment tensor and orientation of fracture planes with respect to the P-axis and T-axis. Moment tensor solution results in two possible fracture planes: Plane 1 and Plane 2 (Left). Beach ball diagram representing a pure strike-slip event corresponding to the shown focal mechanism (Right).

The focal mechanism of a seismic event can be determined from eigenvectors of the event's moment tensor. The three orthogonal eigenvectors of the moment tensor denote a pressure axis (*P*), a tensile axis (*T*), and a null axis (*N*). The slip (fracture) plane is oriented at 45° from the T- and P-axes and contains the N-axis as shown

in Figure 1 (Cronin, 2010). The slip vector on the plane (rake vector) can then be determined using a set of equations relating the slip vector to the fracture normal vector and the moment tensor eigenvectors. More details can be found in Jost and Herrmann (1989).

The focal mechanism provides three important parameters: fracture strike, dip, and rake angle. The fracture strike is measured clockwise from north, ranging from 0 to 360°, with the fracture plane dipping to the right when looking along the strike direction. The dip is measured from horizontal and varies from 0 to 90°. The slip (or rake) vector represents the slip direction of hanging wall relative to foot wall. The rake angle is the angle between the strike direction and the rake vector. It changes from 0 to 180° when measured counterclockwise from strike and from 0 to −180° when measured clockwise from strike (when viewed from the hanging wall side) (Figure 2).

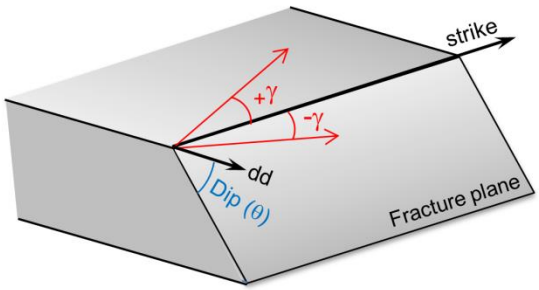

Figure 2: Rake vector and rake angle (γ) on a fracture plane, looking from hanging wall. Rake angle is measured positive counter clockwise and negative clockwise from strike.

An inherent ambiguity in the moment tensor solution is that it provides two possible fracture planes for each seismic event: a real plane and an auxiliary plane that are orthogonal to one another (Figure 1). The auxiliary plane has no physical value and is just the byproduct of the solution. The moment tensor itself does not provide any further information that can be used to distinguish the real plane (Cronin, 2010). The knowledge of the field stress regime can help differentiate the real plane from the auxiliary plane. Since the moment tensor solution is estimated from noisy data, near-vertical slip planes can become problematic. Slight deviations of the estimated dip of the slip plane on either side of vertical can produce an artificially reversed rake vector for some events, meaning that the calculated slip direction is 180° off from the real slip direction. This issue and the auxiliary plane ambiguity must be considered and properly addressed before proceeding to stress calculation from the microseismic focal mechanism. This will be further discussed in the next section.

For microseismicity induced by hydraulic fracturing, an inversion approach is used to find a moment tensor corresponding to each recorded event. In this technique, a best-fit solution is sought by minimizing a residual function, usually a least-squares function, for all wave patterns recorded for a given event by different receivers. Details of moment tensor inversion techniques can be found in Jost and Herrmann (1989), and Dahm and Kruger (2014).

3. STRESS CALCULATION METHOD

The stress calculation method includes two main steps: i) determination of horizontal stress directions, and ii) calculation of maximum horizontal stress magnitude.

Consistent with the common practice in industry, the vertical stress is assumed as a principal stress, implying that the other two principal stresses are horizontal. Provided there are no major structural features, such as a fold or a fault, this assumption is generally valid for most unconventional reservoirs, considering the high depth of the reservoirs and the high magnitude of overburden pressure.

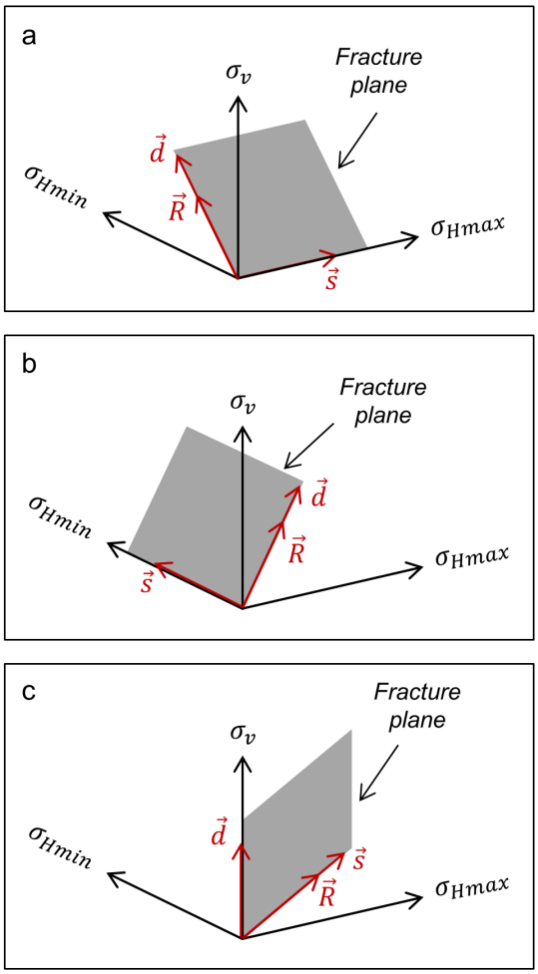

Figure 3: Fracture planes with dip or strike parallel to one of the principal stresses. These fractures cannot be used for stress calculations because their rake vector (***R***) is no longer a function of relative stress magnitudes. The non-vertical fractures with their strike parallel to one of the horizontal stresses (a and b) show a pure dip-slip mechanism and can be used to determine the direction of horizontal stresses.

Assuming the vertical stress is a principal stress, the direction of horizontal stresses can be determined from the focal mechanisms that meet a certain geometric criterion. Based on the principles of solid mechanics the shear vector on a plane (fracture) oriented parallel to a principal stress is always perpendicular to that principal direction. This rule can be used to identify the fractures which are aligned with horizontal stresses. In other words, in a stress field with a vertical principal stress any non-vertical fracture plane with a dip-slip mechanism (rake angle of $\gamma = \pm 90°$) is oriented parallel to one of the horizontal stresses (σ_{Hmax} or σ_{hmin}), as shown in Figure 3. The strikes of these fractures are coincident with the direction of field horizontal stresses.

Having determined the direction of horizontal stresses, the reference coordinate system is formed as a right-handed coordinate system with σ_{Hmax}, σ_{hmin}, and σ_v directions being the first (X_1), second (X_2) and third (X_3) coordinate axes, respectively (Figure 4).

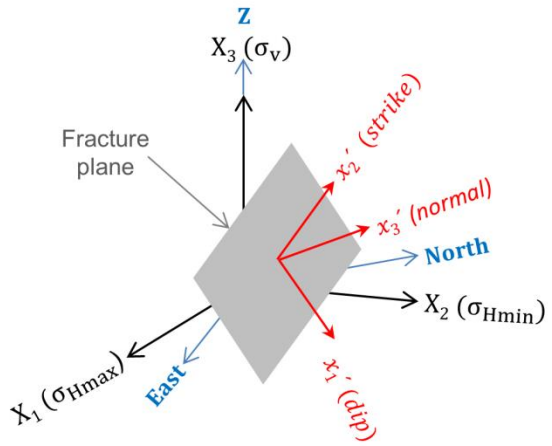

Figure 4: Geographic coordinate system E-N-Z (blue), reference (principal stresses) coordinate system σ_{Hmax}-σ_{hmin}-σ_v (black), and fracture local coordinate system dip-normal-strike (red).

A fundamental assumption in calculating the magnitude of σ_{Hmax} from microseismic focal mechanisms is that the rake vector (slip vector) ($\boldsymbol{R}$), which is determined from moment tensor solution, is parallel with the maximum shear vector acting on the fracture plane ($\boldsymbol{T_s}$), resulting from projection of stress tensor on the fracture plane. This assumption is valid for small slips on planar fractures or undulating fractures that slip under high normal stresses. In the latter case, the fracture asperities will shear off under high normal stress, and the shear displacement will follow the maximum shear force direction (Barton and Choubey, 1977, Patton, 1966). A governing equation is formed by setting the external product of rake ($\boldsymbol{R}$) and shear stress ($\boldsymbol{T_s}$) vectors to zero, as follows:

$$\boldsymbol{R} \times \boldsymbol{T_s} = 0 \tag{2}$$

The components of the rake vector ($\boldsymbol{R}$) in the local coordinate system (primed) of the fracture plane (Figure 4) are:

$$\boldsymbol{R'} = R_1'\boldsymbol{x_1'} + R_2'\boldsymbol{x_2'} + R_3'\boldsymbol{x_3'} \tag{3}$$

$$R_1' = -\sin\gamma \tag{4}$$

$$R_2' = \cos\gamma \tag{5}$$

$$R_3' = 0 \tag{6}$$

where γ is the rake angle (Figure 2).

The components of the rake vector in the reference coordinate system (unprimed) can be determined by using the following transformation rule:

$$\boldsymbol{R} = [A]^T\boldsymbol{R'} \tag{7}$$

where $[\boldsymbol{A}]^{\boldsymbol{T}}$ is the transpose of the transformation matrix $[A]$, whose components are the direction cosines of the primed coordinate axes in the reference (unprimed) coordinate axes. The transformation matrix for each fracture plane has the following form:

$$[A] = \begin{bmatrix} V_{d1} & V_{d2} & V_{d3} \\ V_{s1} & V_{s2} & V_{s3} \\ N_1 & N_2 & N_3 \end{bmatrix} \tag{8}$$

where V_{di}, V_{si}, and N_i are the components of unit dip vector ($\boldsymbol{V_d}$), unit strike vector ($\mathbf{V_s}$), and unit normal vector ($\mathbf{N}$), of the fracture plane, respectively, all in the reference coordinate system. The dip and strike vectors can be written in the reference coordinate system as follows:

$$\boldsymbol{V_s} = \sin\alpha\,\boldsymbol{X_1} + \cos\alpha\,\boldsymbol{X_2} \tag{9}$$

$$\boldsymbol{V_d} = \cos\theta\sin\beta\,\boldsymbol{X_1} + \cos\theta\cos\beta\,\boldsymbol{X_2} - \sin\theta\,\boldsymbol{X_3} \tag{10}$$

where α is the fracture strike angle measured from σ_{hmin} direction (X_2 axis in the reference coordinate system), θ is the fracture dip angle measured from horizontal, and β is the dip direction angle ($\beta = \alpha + 90$). Given the strike of a fracture plane is always measured from true north a correction must be applied to calculate α in Equation 9 if σ_{hmin} direction is not aligned with true north. α can be calculated as:

$$\alpha = s - \omega \tag{11}$$

where s is the fracture strike measured clockwise from north and ω is the rotation angle between σ_{hmin} direction and north. The rotation angle ω can be calculated from the azimuth of σ_{Hmax}, measure clockwise from north, as $\omega = \sigma_{Hmax}$ azimuth – 90°.

The fracture unit normal vector is determined as the external product of dip and strike vectors:

$$\boldsymbol{N} = \boldsymbol{V_d} \times \boldsymbol{V_s} \tag{12}$$

By applying Eq. 7 the rake vector ($\boldsymbol{R}$) in the reference coordinate system is determined as:

$$\boldsymbol{R} = R_1\boldsymbol{X_1} + R_2\boldsymbol{X_2} + R_3\boldsymbol{X_3} \quad (13)$$

$$R_1 = -\sin\gamma\cos\theta\sin\beta + \cos\gamma\sin\alpha \quad (14)$$

$$R_2 = -\sin\gamma\cos\theta\cos\beta + \cos\gamma\cos\alpha \quad (15)$$

$$R_3 = \sin\gamma\sin\theta \quad (16)$$

The stress tensor is formed in the reference coordinate system as follows:

$$\sigma_{ij} = \begin{bmatrix} \sigma_{11} & 0 & 0 \\ 0 & \sigma_{22} & 0 \\ 0 & 0 & \sigma_{33} \end{bmatrix} = \begin{bmatrix} \sigma_{Hmax} & 0 & 0 \\ 0 & \sigma_{hmin} & 0 \\ 0 & 0 & \sigma_v \end{bmatrix} \quad (17)$$

Considering the vertical scatter of induced microseismic events, the components of the stress tensor must be normalized by a depth factor. Assuming vertical stress is $\sigma_v = d \times \sigma_{vGrad}$ where d is depth and σ_{vGrad} is vertical stress gradient, with units of stress/length such as psi/ft or ppg, the stress tensor can be normalized by vertical stress:

$$S_{ij} = \frac{\sigma_{ij}}{\sigma_v} = \begin{bmatrix} k_H & 0 & 0 \\ 0 & k_h & 0 \\ 0 & 0 & 1 \end{bmatrix} \quad (18)$$

where:

$$k_H = \sigma_{Hmax}/\sigma_v$$

$$k_h = \sigma_{hmin}/\sigma_v$$

The main advantage of this formulation is that it eliminates the vertical stress component from the stress calculation equations and leaves k_H and k_h as the only variables.

The traction vector ($\boldsymbol{T}$) acting on the fracture plane is calculated from the stress tensor and fracture normal vector as:

$$T_i = S_{ij}N_j \quad (19)$$

where S_{ij} is the normalized stress tensor (Eq. $S_{ij} = \frac{\sigma_{ij}}{\sigma_v} = \begin{bmatrix} k_H & 0 & 0 \\ 0 & k_h & 0 \\ 0 & 0 & 1 \end{bmatrix}$ (1818), and $\boldsymbol{N}$ is the normal unit vector to fracture plane. This equation gives the traction vector components in terms k_H and k_h. The shear stress vector ($\boldsymbol{T_s}$) on the fracture plane can then be determined as the projection of traction vector on the fracture plane. The components of the shear vector in the reference coordinate system are:

$$T_s = T_{s1}\boldsymbol{X_1} + T_{s2}\boldsymbol{X_2} + T_{s3}\boldsymbol{X_3} \quad (20)$$

$$T_{s1} = \sigma_v N_1\left[N_2{}^2(k_H - k_h) - N_3{}^2(1 - k_H)\right] \quad (21)$$

$$T_{s2} = \sigma_v N_2\left[N_3{}^2(k_h - 1) - N_1{}^2(k_H - k_h)\right] \quad (22)$$

$$T_{s3} = \sigma_v N_3\left[N_1{}^2(1 - k_H) - N_2{}^2(k_h - 1)\right] \quad (23)$$

where N_1, N_2, and N_3 are the components of the fracture normal vector in reference coordinates (Eq. 12).

Substituting rake and shear vectors from Eq. 13 and Eq. 20 in Eq. 2 results in a linear relationship between k_H and k_h for each focal mechanism as below:

$$k_H = M_1 + M_2 k_h \quad (24)$$

The coefficients of Eq. 24 can be calculated from the following equations:

$$M_1 = a_3/a_1 \quad (25)$$

$$M_2 = a_2/a_1 \quad (26)$$

where:

$$a_1 = R_3N_2N_1{}^2 - R_2N_3N_1{}^2 \quad (27)$$

$$a_2 = R_2N_3N_2{}^2 + R_3N_2N_3{}^2 + R_3N_2N_1{}^2 \quad (28)$$

$$a_3 = -R_2N_3N_1{}^2 - R_2N_3N_2{}^2 - R_3N_2N_3{}^2 \quad (29)$$

Equation (24) establishes a linear relationship between the normalized magnitudes of σ_{Hmax} and σ_{hmin} for each event. Provided the magnitudes of σ_{hmin} and σ_v are known (for example, from a mini-frac test and density logs, respectively), k_H and the absolute magnitude of σ_{Hmax} can be calculated for each event.

4. HORIZONTAL STRESS MAGNITUDE

In this method, each qualifying focal mechanism is considered as an independent test for measuring the σ_{Hmax} magnitude. The calculated k_H values for all fractures can be plotted on a histogram for further interpretation and estimation of the undisturbed maximum horizontal stress. Figure 5 shows a histogram of k_H values for a Marcellus well. The formation stress regime is normal faulting with the measured $k_h = \sigma_{hmin}/\sigma_v = 0.675$. It should be noted that for an undisturbed stress state, all k_H values must be theoretically identical and stack on the same bar.

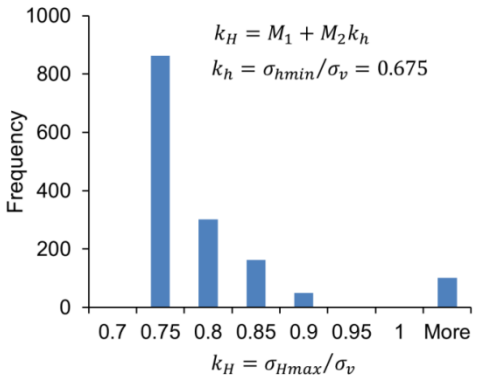

Figure 5: Distribution of calculated k_H values from qualified focal mechanisms for a Marcellus pad with field k_h=0.675.

However, when a hydraulic fracture is created, it changes the field stresses around the open fracture. Numerical simulation of hydraulic fracturing indicates that at least three different stress fields can be identified

around a planar vertical hydraulic fracture (Agharazi et al. 2013, Nagel et al. 2013), as shown in Figure 6: i) the undisturbed zone, ii) the stress-shadow zone on either side of the hydraulic fracture, and iii) the shear zone at the horizontal leading tip of the hydraulic fracture.

Within the shear zone (Zone 3) the stresses rotate and the shear stress magnitude increases. The microseismic events that occur in this zone are mostly dry events (driven by higher shear stress rather than fluid pressure increase) with a higher likelihood of a strike-slip focal mechanism. Neither the stress magnitudes nor the stress directions are representative of the field stresses in this zone. In Figure 5, the events with the calculated $k_H > 1$ do not follow a normal faulting stress state and most likely belong to this zone.

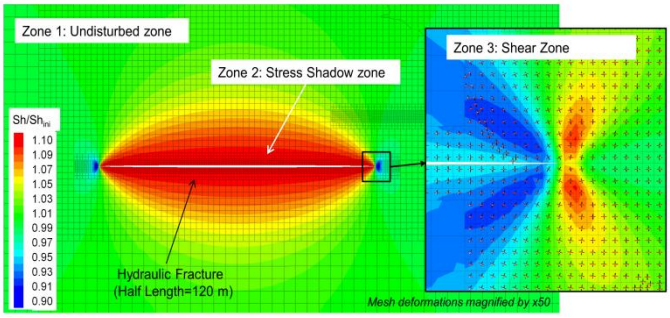

Figure 6**:** In-situ and induced stress zones around a propped-open vertical hydraulic fracture (map view crossing at the center of fracture). The shear zone (Zone 3) forms at the leading tip of hydraulic fractures. Both stress directions and magnitudes are altered in this zone. The stress-shadow zone (Zone 2) develops on the other side of the fracture and features higher compressive stress in the direction normal to the fracture plane (usually σ_{hmin} direction). In this zone, the stress directions remain mainly unchanged. Outside of these two zones, stresses are not changed and represent the initial field stresses (Zone 1).

In the stress-shadow zone (Zone 2), however, the direction of stresses remain unchanged, but the magnitude of the stress component acting normal to the fracture plane (usually σ_{hmin}) increases due to dilation of the fracture and deformation of rock. Microseismic events with the hypocenters located in this zone results in higher apparent k_H values, consistent with the higher k_h values in this zone (note the linear relationship between k_H and k_h). These events can be used to track the stress disturbances around an induced hydraulic fracture. Most microseismic events in this zone are wet events, mainly because the increase of fluid pressure is the only factor that can trigger failure under higher σ_{hmin} (less shear stress) in this zone. Numerical studies show that for a vertical planar fracture, the maximum theoretical extension of the stress-shadow zone is equal to one fracture height on either side of the fracture in an elastic fracture-free rock (Agharazi et al., 2013). In Figure 5, shorter bars with higher k_H values potentially represent the events with hypocenters located in the stress shadow zone.

Finally, outside of these two zones (Zone 1), either the stress magnitudes or the stress directions are undisturbed and represent the initial field stresses. Considering the limited extension of the two previous zones and large spatial scatter of microseismic events, a higher population of the events falls into this zone and can be used to back-calculate the undisturbed maximum horizontal stress (the tallest bar in Figure 5).

For the case shown in Figure 5 an upper limit k_H value can be calculated by averaging all $k_H < 1$ (all normal faulting events), while a more representative value can be calculated by just averaging the k_H values between $0.7<k_H<0.75$, which more likely represent the undisturbed σ_{Hmax} value. Other factors such as quality of microseismic events, defined as signal-to-noise ratio (SNR) and uncertainty of moment tensor solution, can also be included at this stage for a more precise interpretation of stress calculation results.

5. DISCUSSION

The coefficients of linear relationship between k_H and k_h (Eq.24), M_1 and M_2, are solely functions of fracture strike, dip, and rake with respect to the reference coordinate system and are independent of stress magnitudes. In other words, these coefficients can be calculated once the direction of horizontal stresses is determined and the reference coordinate system is established. An important characteristic of these coefficients is that they follow a sign convention corresponding to the stress regime that governs the slip mechanism on the fracture plane. Table 1 lists the M_1 and M_2 signs corresponding to three possible stress regimes.

Table 1: Signs of M_1 and M_2 for three possible stress regimes

Stress Regime	Stress State $\sigma_3<\sigma_2<\sigma_1$	Normalized stresses	M_1	M_2
Normal Faulting	$\sigma_{hmin}<\sigma_{Hmax}<\sigma_v$	$k_h<k_H<1$	+	+
Strike Slip	$\sigma_{hmin}<\sigma_v<\sigma_{Hmax}$	$k_h<1<k_H$	+	−
Reverse Faulting	$\sigma_v<\sigma_{hmin}<\sigma_{Hmax}$	$1<k_h<k_H$	−	+

Table 1 can be consulted as a guide for quality control of moment tensor solution results and identifying the incompatible focal mechanisms with respect to the field stresses. For example, if the hydraulic fracturing stimulation is carried out in a formation with known $k_h < 1$ (normal faulting or strike-slip) the fractures with $M_1 < 1$ indicate inconsistency with the stress field and must be tagged as incompatible focal mechanisms.

Using this approach, the real nodal plane can be differentiated from the auxiliary nodal plane before back-calculating the stresses. The potential error in the dip direction for near-vertical fractures can also be identified and addressed in the same way.

An important step in this method is identifying and filtering out the fractures that do not qualify for stress calculation. For any stress field, the unqualified fractures are those whose strike or dip vector is parallel to one of the principal stress directions (Figure 3). For these cases, the principal stress parallel to the strike or dip vector of the fracture has no projection on the fracture plane and does not affect the shear vector direction. The shear vector falls in the plane normal to that principal stress component irrespective of the relative magnitudes of principal stresses. For these fractures, any combination of stress magnitudes satisfies the governing equation (Eq. 2), which implies non-uniqueness of the solution for these fractures. These fractures can be identified once the reference coordinate system of principal stress directions is established and must be eliminated from stress calculations; however, as shown in Figure 3, most of the unqualified focal mechanisms for stress calculations are the ones that are used for determination of horizontal stress direction.

The potential polarity issue in the calculated rake vector direction is automatically addressed by the chosen governing equation (Eq. 2). Considering the external product of two parallel vectors is always zero, this equation is satisfied as long as rake vector ($\boldsymbol{R}$) is aligned with shear vector ($\boldsymbol{T_s}$), irrespective of its direction.

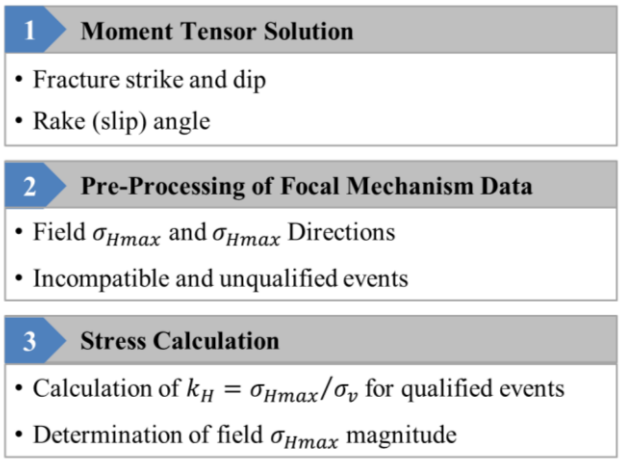

Figure 7: Three main steps to calculate maximum horizontal stress direction and magnitude from microseismic focal mechanisms.

The pre-processing and quality control of the focal mechanisms, resulting from moment tensor solutions, is a critical step that must be taken before proceeding to the stress calculation step. Existence of any unqualified or incompatible focal mechanism in the data set under investigation potentially results in a significant scatter in the calculated k_H values and consequently a considerable error in the estimated field σ_{Hmax}. Figure 7 shows the main steps of stress calculation using the suggested method.

6. CASE STUDIES

We studied two Marcellus projects, Project A and Project B, including three and two horizontal wells in a pad, respectively. The projects are located about 30 miles away from each other. The Marcellus shale is a black shale unit of the Hamilton group of the Middle Devonian section of the Appalachian Basin. The fracture system is mainly characterized by two systematic sub-vertical joint sets, *J1* and *J2*. In the Marcellus, the *J1* fractures predominate and are more closely spaced. They strike east-northeast sub-parallel to maximum horizontal compressive stress**.** The *J2* fractures generally crosscut *J1* fractures (Engelder et al. 2009).

Consistent with the industry common practice in the Marcellus, all study wells were drilled parallel to the general direction of the minimum horizontal stress in the basin (northwest-southeast). The vertical stress gradient was calculated from density logs and ranges between 1.17 and 1.2 psi/ft. The minimum horizontal stress gradient ranges between 0.79 and 0.82 psi/ft.

Project A included three wells with an average lateral length of 6000–7000 ft. All wells were completed using a plug-and-perf completion technique and slickwater. The average stage length was 170 ft. Each well was completed independently after the completion of the previous well. Figure 8 shows the distribution of the induced microseismic events recorded during the treatments.

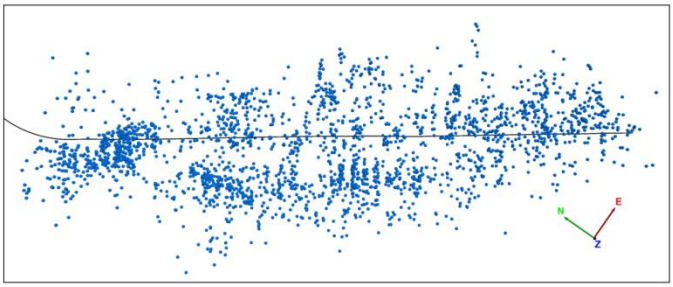

Figure 8: Distribution of microseismic events in Project A (looking down from surface). Only the middle well is shown with a length of 6500 ft.

In total, 2,830 microseismic events with signal-to-noise ratios of SNR>7 were recorded for this project. The σ_{Hmax} direction was determined as N050° from 184 focal mechanisms that met the stress direction criterion (Figure 3). The stress calculation was performed based on 2123 qualified events, which resulted in the following relationship between k_H and k_h:

$$k_H = 0.22 + 0.78k_h \quad (30)$$

For a vertical stress gradient of σ_v =1.20 psi/ft and minimum horizontal stress gradient of σ_{hmin}= 0.81 psi/ft, Equation 30 results in a maximum horizontal stress of σ_{Hmax}= 0.896 psi/ft.

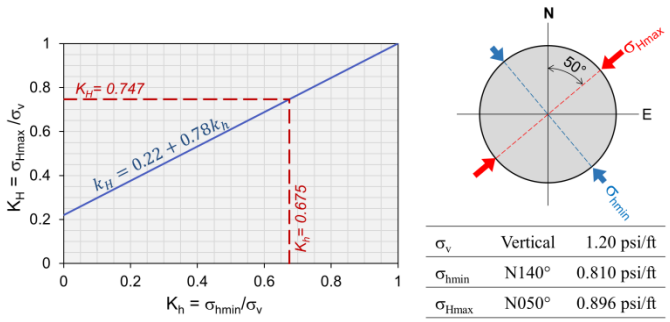

σ_v	Vertical	1.20 psi/ft
σ_{hmin}	N140°	0.810 psi/ft
σ_{Hmax}	N050°	0.896 psi/ft

Figure 9: Calculated maximum horizontal stress magnitude and direction for Project A in the Marcellus Shale. The plot on the left shows the obtained linear relationship between k_H and k_h. The normalized σ_{Hmax} is calculated as $k_H = 0.747$ for the field $k_h = 0.675$. The maximum horizontal stress direction and gradient were determined as N050° and 0.896 psi/ft, respectively.

At the treatment depth of 7,300 ft, the horizontal stress anisotropy was calculated equal to $\sigma_{Hmax} - \sigma_{hmin}$= 560 psi. Figure 10 shows the Mohr circles corresponding to the calculated field (undisturbed) stresses in the Marcellus and the initial state of stress on the stimulated fractures recorded by microseismic monitoring.

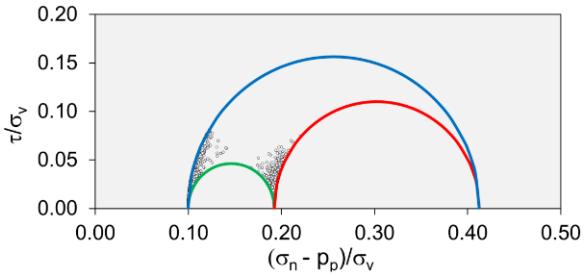

Figure 10: Mohr circles showing the calculated undisturbed state of stress for Project A in the Marcellus. The black dots indicate the initial state of stress on stimulated fractures.

In the second project (Project B) all wells were also completed using the plug-and-perf method and slickwater. In total, 710 microseismic events were recorded during all stages of the treatment. The vertical stress gradient was estimated as σ_v=1.18 psi/ft, and minimum horizontal stress was σ_{hmin}=0.79 psi/ft for the pad. In this case, the stress calculation is performed based on the microseismic events collected from one well, i.e., 400 events out of 710 total events. It demonstrates a case where σ_{Hmax} is estimated at a smaller scale (well scale) versus the previous case, where σ_{Hmax} was determined at a larger scale (pad scale). Out of 400 focal mechanisms collected for the study well, 32 events were used to determine the σ_{Hmax} direction and 357 events were qualified for stress calculation. The remaining 11 events met neither the direction criterion nor the stress calculation criterion, and hence were eliminated. Figure 11 shows the results of stress calculation for this well.

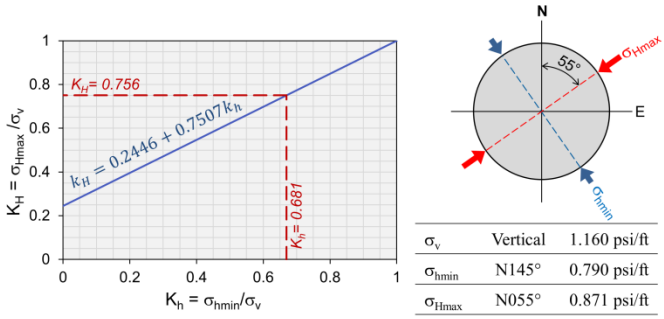

σ_v	Vertical	1.160 psi/ft
σ_{hmin}	N145°	0.790 psi/ft
σ_{Hmax}	N055°	0.871 psi/ft

Figure 11: Calculated maximum horizontal stress magnitude and direction for Project B in the Marcellus Shale. The plot on the left shows the obtained linear relationship between k_H and k_h. The normalized σ_{Hmax} is calculated as $k_H = 0.756$ for the field $k_h = 0.681$. The maximum horizontal stress direction and gradient were determined as N055° and 0.871 psi/ft, respectively.

The horizontal stress anisotropy at the target depth of 6,300 ft was calculated as $\sigma_{Hmax} - \sigma_{hmin} = 547$ psi. The calculated stress magnitudes and directions for both projects show a good consistency. Considering the close proximity of these two projects (~30 miles) these results were expected. In both case studies, the stress calculation indicates a normal faulting stress regime that is consistent with our knowledge of stress state in the study area. Figure 12 shows the Mohr circle representation of the field stress state, along with the initial state of stress on stimulated fractures for this well.

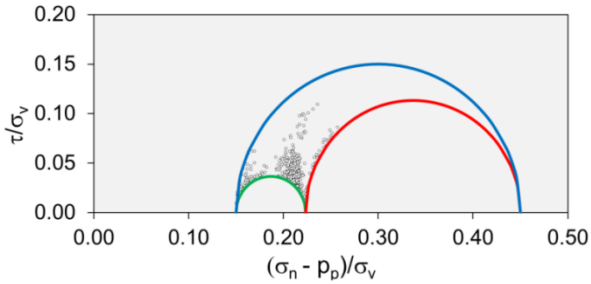

Figure 12: Mohr circles showing the calculated undisturbed state of stress for Project B in the Marcellus. The black dots indicate the initial state of stress on stimulated fractures.

7. CONCLUSION

A deterministic method was introduced for estimation of maximum horizontal stress direction and magnitude based on microseismic focal mechanisms. In this method, each qualified microseismic focal mechanism is treated as an independent field test that can be used for determination of either σ_{Hmax} direction or its magnitude. Considering the scatter of microseismic events over a relatively large area, the estimated stress magnitude well

represents the field stresses at a large scale, as opposed to other indirect methods such as borehole breakout analysis, which is more representative of local stresses around the study well. This method can also be used to isolate the zones with perturbed stresses, induced either by hydraulic fracturing or related to a geological feature such as a fault.

The proposed method has several significant advantages over the stress inversion techniques for stress estimation from microseismic focal mechanisms. It determines horizontal stress direction independently before stress calculation, hence, at the stress calculation step, it solves one equation for one unknown that guarantees the uniqueness of the solution. The adopted formulations in this method allow quality control of moment tensor solutions and identifying and addressing the incompatible or unqualified events, which otherwise would cause a significant error in the calculations.

Since both the suggested stress calculation method in this paper, and the moment tensor solution used to determine microseismic focal mechanisms are purely mathematical and deterministic processes, the accuracy of the calculated stress parameters directly depends on the certainty level of moment tensor inversions. The lower the uncertainty of moment tensor inversion, the higher the accuracy of moment tensor solutions and the higher the quality of calculated focal mechanisms.

The suggested method was successfully applied to two projects in the Marcellus, and the magnitude and direction of maximum horizontal stresses were calculated.

REFERENCES

1. Agharazi, A., B. Lee, N.B. Nagel, F. Zhang, M. Sanchez, 2013. Tip-Effect Microseismicity – Numerically Evaluating the Geomechanical Causes for Focal Mechanisms and Microseismicity Magnitude at the Tip of a Propagating Hydraulic Fracture. In *Proceedings of the SPE Unconventional Resources Conference Canada, Calgary, 5-7 November 2013*
2. Amadei B., O. Stephansson, 1997. *Rock Stress and Its Measurement*. London: Chapman & Hall
3. Angelier, J., 1990. Inversion of Field Data in Fault Tectonics to Obtain the Regional Stress, A New Rapid Direct Inversion Method by Analytical Means, *Geophys. J. Int*., 103, 363-376.
4. Barton, N., V. Choubey, 1977. The shear strength of joints in theory and in practice. *Rock Mech*., 10,: 1-65.
5. Cronin, V., 2010. A Primer on Focal Mechanism Solutions for Geologists. Science Education Resource Center, Carleton College, *accessible via http://serc.carleton.edu/files/ NAGTWorkshops/structure04/Focal_mechanism_primer.pdf*
6. Dahm, T., F. Kruger, 2014, Moment tensor inversion and moment tensor interpretation. In *New Manual of Seismological Observatory Practice 2 (NMSOP-2),* ed. Bormann P. 1-37
7. Engelder, T., G.G. Lash, R.S. Uzcategui, 2009. Joint sets that enhance production from Middle and Upper Devonian gas shales of the Appalachian Basin. *The American Association of Petroleum Geologists Bulletin,* 93(7)857-889
8. Gephart, J.W., D.W. Forsyth, 1984. An Improved Method for Determining the Regional Stress Tensor Using Earthquake Focal Mechanism Data - Application to the San-Fernando Earthquake Sequence, *J. Geophysics Res*., 89: 9,305-9,320.
9. Jaeger, J.C., N.G.W. Cook, R.W. Zimmerman, 2008. *Fundamentals of Rock Mechanics*. 4th ed. Malden: Blackwell Publishing
10. Jost, M.L., R.B. Herrmann. 1989. A Student's Guide to and Review of Moment Tensors. *Seismological Research Letters*, 60(2), 37-57
11. Michael, A.J., 1984. Determination of stress from slip data: Faults and folds, *J. Geophys. Res*., 89: 11,517-11,526.
12. Nagel, N.B., M. Sanchez-Nagel, F. Zhang, X. Garcia, B. Lee, 2013. Coupled Numerical Evaluations of the Geomechanical Interactions Between a Hydraulic Fracture Stimulation and a Natural Fracture System in Shale Formation. *Rock Mech Rock Eng* 46:581-609.
13. Neuhaus, C.W., S. Williams, C. Remington, B.B. William, K. Blair, G. Neshyba, T. McCay. 2012. Integrated Microseismic Monitoring for Field Optimization in the Marcellus Shale – A Case Study. In *Proceedings of the SPE Canadian Unconventional Resources Conference, Calgary, 30 October – 1 November 2012*
14. Patton, F.D. 1966. Multiple modes of shear failure in rock. In *Proceeding of 1th International Congress of International Society for Rock Mechanics, Lisbon, 23-24 October,* (1) 509-513.
15. Sasaki, S., H. Kaieda, 2002. Determination of Stress State from Focal Mechanisms of Microseismic Events Induced During Hydraulic Injection at the Hijiori Hot Dry Rock Site, Pure appl. geophys. 159, 489-516
16. Sinha, B.K., J. Wang, S. Kisra, J.Li, V. Pistre, T. Bratton, M. Sanders, C. Jun. 2008. In *Proceedings of 49th Annual Logging Symposium, Austin, 25-28 May 2008*
17. Zoback M.D., 2010. *Reservoir Geomechanics*. 1st ed. New York: Cambridge University Press